viable means of sensing CO in the present case, the use of a more conducting matrix is in order. To this end, we are currently investigating the incorporation of [Rh(TMPP)$_2$(CO)][BF$_4$] (1) into solid ionic conducting polymer films such as MEEP (poly[bis(2-(2-methoxy)ethoxy)phosphazene]).[8]

These studies demonstrate that the molecular cationic complex [Rh(TMPP)$_2$(CO)]$^+$ (1) reversibly binds CO within a glassy polymer matrix to form the dicarbonyl species [Rh(TMPP)$_2$(CO)$_2$]$^+$ (2). The facile nature of the chemistry is a direct consequence of an exceedingly labile metal–methyl, phenyl ether bond, which facilitates substitution reactions even in the solid state. The addition of CO conveniently gives rise to dramatic changes in the spectroscopic and redox properties of the rhodium cation, commensurate with coordination of a strong π-acceptor to the metal center. On the basis of these preliminary results with titania and zirconia films incorporating [Rh(TMPP)$_2$(CO)][BF$_4$] (1), the development of other CO sensing films using molecular composites of ether–phosphine complexes appears attractive.

Acknowledgment. We gratefully acknowledge the National Science Foundation (P.I. Grant CHE-8914915 to K.R.D.) and Camille and Henry Dreyfus Foundation (Teacher-Scholar award to K.R.D.) for financial support. We also gratefully acknowledge the Michigan State University College of Natural Science and The Dow Chemical Co. for providing research fellowships for S.C.H. Support was also provided by the Crop and Food Bioprocessing Center at Michigan State University for J.I.D. and the Cooperative State Research Service (CSRS) of the United States Department of Agriculture (grant to K.A.B.).

(7) Mirkin, C. A.; Wrighton, M. S. *J. Am. Chem. Soc.* **1990**, *112*, 8596.
(8) (a) Allcock, H. R.; Austin, P. E.; Neenan, T. X.; Sisko, J. T.; Blonsky, P. M.; Shriver, D. F. *Macromolecules* **1986**, *19*, 1508. (b) Blonsky, P. M.; Shriver, D. F.; Austin, P. E.; Allcock, H. R. *Solid State Ionics* **1986**, *18*, 258. (c) Blonsky, P. M.; Shriver, D. F.; Austin, P. E.; Allcock, H. R. *J. Am. Chem. Soc.* **1984**, *106*, 6854. (d) Austin, P. E.; Riding, G. J.; Allcock, H. R. *Macromolecules* **1983**, *16*, 719.

A Sol–Gel-like Route to Crystalline Cadmium Phosphide Nanoclusters

Michael A. Matchett,[1] Ann M. Viano,[2] Natalie L. Adolphi,[2] R. Dean Stoddard,[2] William E. Buhro,*[,1] Mark S. Conradi,*[,2] and Patrick C. Gibbons*[,2]

Departments of Chemistry and Physics
Washington University
St. Louis, Missouri 63130

Received January 28, 1992
Revised Manuscript Received April 8, 1992

Herein we describe a metalloorganic route to semiconductor nanoclusters[3] that is analogous to the sol–gel process. Our method was designed to parallel the variant of sol–gel processing that affords monodispersed *oxide* particles by the controlled *hydrolysis* and polycondensation of *alkoxide* precursors (see eq 1).[4] By analogy, we proposed the growth of *phosphide* nanoclusters by *alcoholysis* and polycondensation of *disilylphosphido* precursors (see eq 2).[5] The first success of our strategy is the synthesis of soluble, crystalline, cadmium phosphide nanoclusters (nano-Cd$_3$P$_2$).

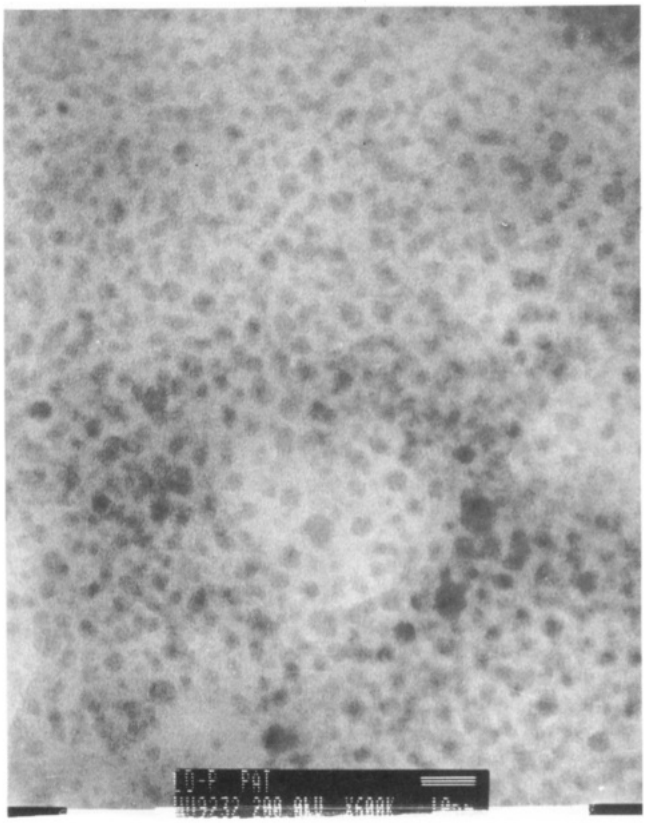

Figure 1. TEM image of Cd_3P_2 nanoclusters obtained from eq 3 and deposited on an amorphous carbon substrate. The striped bar is 100 Å in length.

$$M(OR)_n + nH_2O \xrightarrow[-n\text{ROH}]{\text{hydrolysis}} M(OH)_n \xrightarrow[-n/2H_2O]{\text{polycondensation}} MO_{n/2} \quad (1)$$

$$M\left(P(SiR'_3)_2\right)_n + 2n\text{ROH} \xrightarrow[-2nR'_3SiOR]{\text{alcoholysis}} M(PH_2)_n \xrightarrow[-2n/3PH_3]{\text{polycondensation}} MP_{n/3} \quad (2)$$

The nano-Cd$_3$P$_2$ was prepared from the new disilylphosphido precursor Cd[P(SiPh$_3$)$_2$]$_2$.[6] Initial studies re-

(1) Department of Chemistry.
(2) Department of Physics.
(3) Reviews on semiconductor nanoclusters: (a) Brus, L. *New J. Chem.* **1987**, *11*, 123. (b) Henglein, A. *Chem. Rev.* **1989**, *89*, 1861. (c) Steigerwald, M. L.; Brus, L. E. *Annu. Rev. Mater. Sci.* **1989**, *19*, 471. (d) Stucky, G. D.; Mac Dougall, J. E. *Science* **1990**, *247*, 669. (e) Steigerwald, M. L.; Brus, L. E. *Acc. Chem. Res.* **1990**, *23*, 183. (f) Wang, Y.; Herron, N. *J. Phys. Chem.* **1991**, *93*, 525.

(4) Brinker, C. J.; Scherer, G. W. *Sol-Gel Science*; Academic: New York, 1990; pp 272–284.
(5) Theopold and co-workers were the first to report preparations of semiconductor nanoclusters (nano-GaAs[5a] and nano-InP[5b]) that employed alcoholyses of disilylarsenido and disilylphosphido precursors. Their precursors are of the type R$_2$M–E(SiMe$_3$)$_2$ (where R = alkyl, M = Ga or In, and E = As or P) and involve alkane eliminations along the pathway to nanocluster formation; our precursors do not involve alkane eliminations. Consequently, the pathways are significantly different and the strategies are complementary. (a) Byrne, E. K.; Parkanyi, L.; Theopold, K. H. *Science* **1988**, *241*, 332. (b) Douglas, T.; Theopold, K. H. *Inorg. Chem.* **1991**, *30*, 596.
(6) Cd[P(SiPh$_3$)$_2$]$_2$ was prepared in 95% yield from Cd[N(SiMe$_3$)$_2$]$_2$[6a] and LiP(SiPh$_3$)$_2$·2THF[6b] and was recrystallized from toluene. Satisfactory elemental analyses were obtained (C, H, Cd). ^{31}P NMR (ppm, pyridine) −289.7 (s, satellites 25% intensity, $^1J_{^{31}P-^{111,113}Cd}$ = 774 Hz). The crystal structure has been solved; Cd[P(SiPh$_3$)$_2$]$_2$ is a two-coordinate monomer (Matchett, M. A.; Chiang, M. Y.; Buhro, W. E., unpublished). (a) Bürger, H.; Sawodny, W.; Wannagat, U. *J. Organomet. Chem.* **1965**, *3*, 113. (b) LiP(SiPh$_3$)$_2$·2THF was prepared from P(SiPh$_3$)$_2$[6c] and *n*-BuLi in THF and isolated as a solid by evaporating the volatiles and washing the residue with hexane. ^{31}P NMR (ppm, toluene) −321.2 (s). (c) Hassler, K. *Monatsh. Chem.* **1982**, *113*, 421.

0897-4756/92/2804-0508$03.00/0

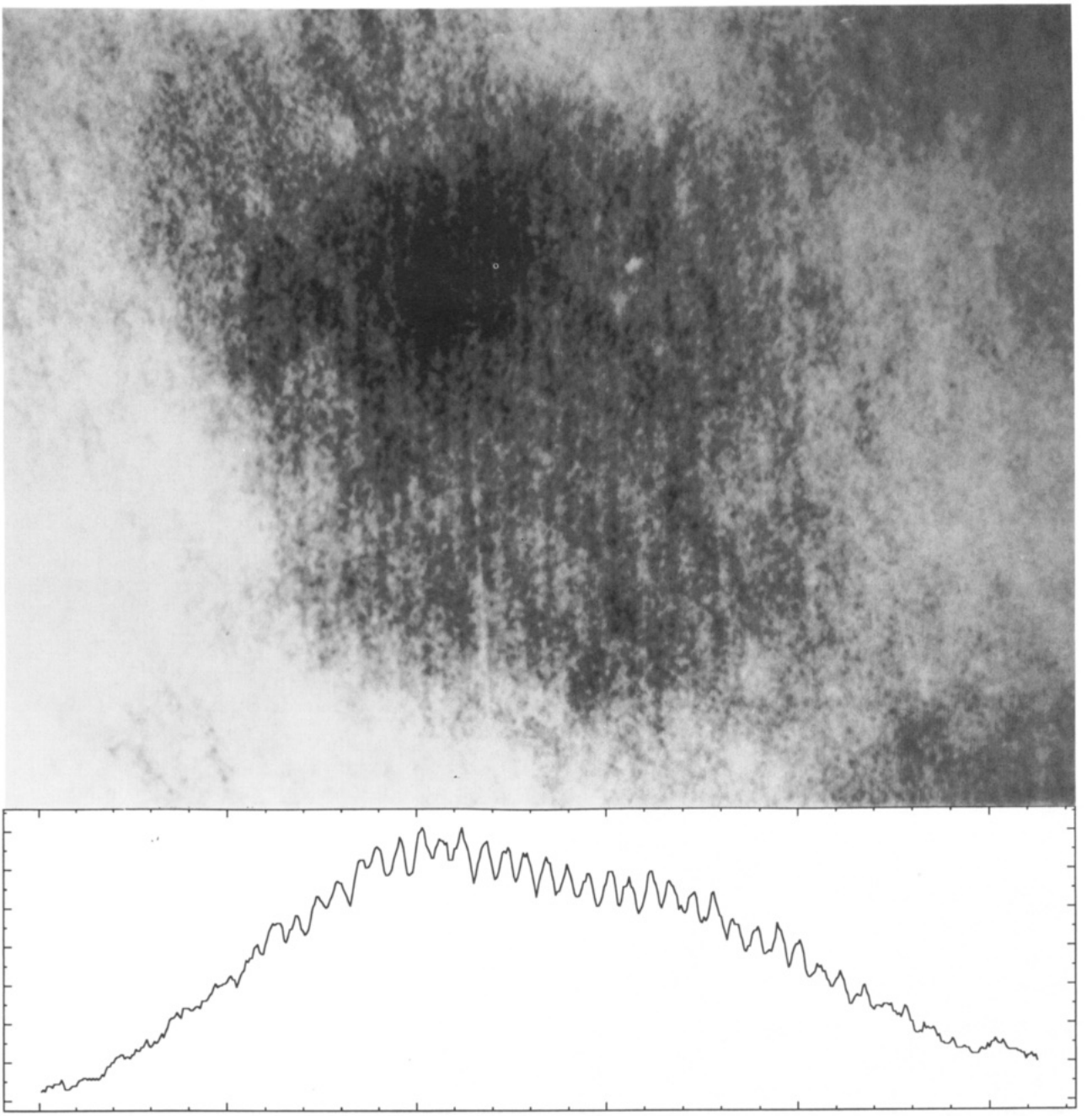

Figure 2. Top: enlargement of a particle from Figure 1 showing lattice fringes. Note a second overlapping particle on the upper left. Bottom: Contrast profile of the particle emphasizing the fringe pattern.

vealed that methanolysis with 4 mol of MeOH/mol of precursor at room temperature in toluene followed instead the stoichiometry given in eq 3 (3–4 days). Under the best

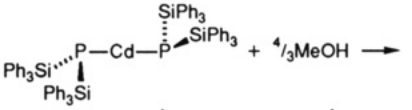

$$^{4}/_{3}\text{-}x\,HP(SiPh_3)_2 + {}^{4}/_{3}\text{-}y\,MeOSiPh_3 + \text{nano-}Cd_3P_2 \quad (3)$$

conditions methanolysis was carried out with 1.33 mol of MeOH/mol of precursor in pyridine. At room temperature the intermediate $Cd[P(SiPh_3)_2][PH(SiPh_3)]$[7] formed by reaction of a single P–$SiPh_3$ bond in the precursor. The temperature was then raised to 60 °C for 15 h, whereupon the homogeneous solution darkened to deep red and nano-Cd_3P_2 formed according to eq 3. The quantities x and y in eq 3 were undetermined and correspond to the –$SiPh_3$ and –OMe groups retained in the nano-Cd_3P_2 (see below). Product isolation was completed by (1) cooling the reaction solution, (2) adding excess MeOH to decompose the $HP(SiPh_3)_2$ byproduct, (3) evaporating the volatiles, and (4) washing the residue with CH_2Cl_2 to remove byproducts (largely $MeOSiPh_3$). The resulting very dark solid, nano-Cd_3P_2, was readily soluble (dispersable) in pyridine but not in other common organic solvents.

The solution-phase and solid-state ^{31}P NMR data for the isolated solid, nano-Cd_3P_2, were consistent with nanoclusters of Cd_3P_2. The solution-phase spectrum exhibited a single, broad, featureless resonance at –240 ppm relative to 85% H_3PO_4 ($\nu_{1/2}$ = 100 ppm), which was upfield of the chemical shifts exhibited by bulk Cd_3P_2 (–140, –162, and –178 ppm).[8] Nanoclusters are expected to exhibit

(7) ^{31}P NMR data for $Cd[P(SiPh_3)_2][PH(SiPh_3)]$ (ppm relative to 85% H_3PO_4, pyridine, in situ): –289.4 (d, $^{1}J_{^{31}P\text{-}^{1}H}$ = 178 Hz; with satellites of 25% intensity, $^{1}J_{^{31}P\text{-}^{111,113}Cd}$ = 507 Hz), –295.4 (s, with satellites of 25% intensity, $^{1}J_{^{31}P\text{-}^{111,113}Cd}$ = 736 Hz).

upfield shifts as a result of a reduction in the paramagnetic-shift term due to the increased bandgap.[9] The breadth of the observed resonance was presumably due to both a distribution of chemical sites within the nanoclusters and a distribution of nanocluster sizes (see below). Exposure of the particles to air gave an additional broad resonance, centered near 0 ppm and assignable to P(V) species.

The solid-state magic-angle-spinning spectrum (−227 ppm, $\nu_{1/2}$ = 88 ppm) closely resembled the solution-phase spectrum, thus verifying that the nanoclusters were precipitated from solution without gross structural changes. The ^{31}P T_2 was also measured, by spin echoes on nonspinning samples. Because under these conditions the dipolar interactions between the ^{31}P nuclei were not refocused by the second pulse, the T_2 was determined by the P–P interaction. Thus T_2 was a measure of the average distance between nearest P atoms and the number of nearest P neighbors. The observed T_2's of 400–460 μs were close to those of bulk Cd_3P_2 (560–600 μs) and indicated that the local structure in nano-Cd_3P_2 was similar to that of the bulk. Specifically, linear or sheetlike polymeric structures for nano-Cd_3P_2 (which require fewer neighbors and consequently yield longer T_2's) were ruled out.

Direct evidence for the particulate nanostructure of nano-Cd_3P_2 was obtained by transmission electron microscopy (TEM). An image of nanoclusters deposited onto a sample grid from solution is shown in Figure 1. This representative sample contained approximately spherical nanoclusters having diameters mostly in the range of 30–40 Å, but with some as small as ca. 20 Å and some as large as ca. 70 Å. Distinct lattice fringes were evident in at least four particles from Figure 1; in these the lattice-fringe patterns extended over the entire particle dimensions (see Figure 2). An electron-diffraction pattern obtained from the sample was well-resolved and corresponded closely to the pattern from bulk Cd_3P_2 (Figure 3, included as supplementary material), indicating that the nanoclusters and bulk Cd_3P_2 shared the same crystalline structure.

The small particle sizes resulted in greatly broadened X-ray diffraction (XRD) patterns (see Figure 4, included as supplementary material), from which an average coherence length of ca. 20 ± 5 Å was calculated from the Scherrer equation.[10,11] The apparent difference between this coherence length and the sizes of the particles in TEM images is probably small compared to experimental uncertainties. However, if the difference is real it *may* suggest (1) that only a fraction of the particles were actually crystalline, (2) that the crystalline domains within individual nanoclusters were on average smaller than the full nanocluster dimensions, or (3) that the particles underwent electron-beam annealing and crystallization in the TEM. The whole-particle extent of the observed lattice-fringe patterns (see above) *might* argue against the second possibility. The third possibility seems unlikely because we detected no time-dependent changes in images or electron-diffraction patterns during and following initial electron-beam exposure.

The nano-Cd_3P_2 retained large numbers of organic residues as surface substituents. Chemical analysis revealed a significant organic fraction (34% C and 41% Cd; cf. 84% Cd for bulk Cd_3P_2).[12] This was confirmed by solid-state ^{31}P NMR spin counting, in which the signal intensity for nano-Cd_3P_2 was only 0.6 of the intensity of an equal mass of pure Cd_3P_2. Thermal decomposition of solid nano-Cd_3P_2 in a sealed tube (180–350 °C) gave bulk Cd_3P_2, P_4, and two organic products, $(Ph_3Si)_2O$ and $MeOSiPh_3$.[13] The origin of $(Ph_3Si)_2O$ was not established; however, we infer that $MeOSiPh_3$ was a primary decomposition product resulting from thermal eliminations of surface –OMe and $-SiPh_3$ substituents. As depicted in cartoon I, we presume that the –OMe groups were bound

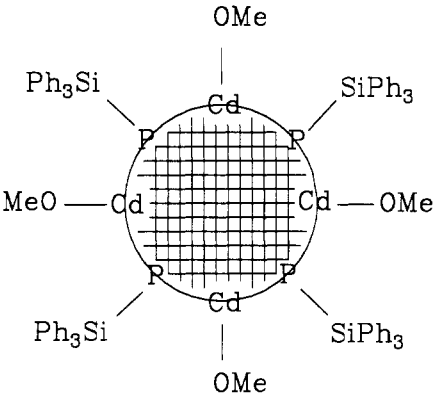

I

to surface cadmium atoms and the $-SiPh_3$ groups to surface phosphorus atoms. Because the surface fraction corresponding to the observed size distribution (see above) in the nanoclusters was large, ca. 40%, a large number of residual organic groups was required to covalently saturate the surfaces and to thereby stabilize the nanoclusters.

The precise nature of the particle-surface structure and capping-group coverage is unknown. The solubility properties of nano-Cd_3P_2 (see above) suggested that surface cadmium atoms were sufficiently exposed to accommodate coordination by the pyridine solvent.[14] Despite stabilization by the covalent surface groups and (likely) solvent ligands, the particles were only metastable; nano-Cd_3P_2 flocculated and precipitated from refluxing pyridine (ca. 12 h). No increase in the XRD coherence length was observed for a sample heated at 100 °C in pyridine for 48 h. nano-Cd_3P_2 also decomposed to insoluble, amorphous Cd_3P_2 when exposed to excess MeOH at ca. 50 °C in solution. In both cases decomposition likely resulted from disruption of the particle-surface ligation.

In a preceding study we described the methanolysis (eq 2) of a related disilylphosphido precursor, $\{Cd[P(SiMe_3)_2]_2\}_2$, which proceeded in a runaway, uncontrolled manner to give insoluble, amorphous Cd_3P_2 rather than soluble nanoclusters.[15] In the present study the effects of changing the silyl substituent in the precursor (from $SiMe_3$ to $SiPh_3$) were a decrease in the rate of the alcoholysis reaction and an alteration in the stoichiometry of the reaction (compare eqs 2 and 3). The altered stoi-

(8) Adolphi, N. L.; Stoddard, R. D.; Goel, S. C.; Buhro, W. E.; Gibbons, P. C.; Conradi, M. S. Submitted to *J. Phys. Chem. Solids.*

(9) (a) Thayer, A. M.; Steigerwald, M. L.; Duncan, T. M.; Douglass, D. C. *Phys. Rev. Lett.* **1988**, *60*, 2673. (b) Mac Dougall, J. E.; Eckert, H.; Stucky, G. D.; Herron, N.; Wang, Y.; Moller, K.; Bein, T.; Cox, D. M. *J. Am. Chem. Soc.* **1989**, *111*, 8006.

(10) Klug, H. P.; Alexander, L. E. *X-Ray Diffraction Procedures*; Wiley: New York, 1974; p 687.

(11) We could not calculate a coherence length from the electron diffraction data because we employed film detection, which recorded intensities according to an unknown nonlinear function.

(12) Analysis of nano-Cd_3P_2 (weight percent): Cd, 41.43; C, 34.06; H, 2.67; N, 1.08. Theory for bulk Cd_3P_2: Cd, 84.47.

(13) The solid-state thermolysis of 260 mg of nano-Cd_3P_2 under the described conditions gave 58 mg (0.11 mmol) of $(Ph_3Si)_2O$ and 25 mg (0.09 mmol) of $MeOSiPh_3$.

(14) We thank a reviewer for suggesting this interpretation.

(15) Goel, S. C.; Chiang, M. Y.; Buhro, W. E. *J. Am. Chem. Soc.* **1990**, *112*, 5636.

chiometry resulted in the retention of both $-SiR_3$ and $-OMe$ groups in quantities high enough to stabilize nanometer-sized particles. Indeed, when the original precursor $\{Cd[P(SiMe_3)_2]_2\}_2$ was reexamined according to the altered stoichiometry of eq 3, soluble nanoclusters were also obtained.[16] We conclude that residual, covalent, surface-capping $-SiR_3$ and $-OMe$ substituents were responsible and necessary for arresting particle growth in the nanometer regime.

A separate route to Cd_3P_2 nanoclusters has been described by Henglein and co-workers.[17] In Henglein's procedure the precipitation of Cd_3P_2 from aqueous solutions of cadmium ions and PH_3 is arrested with the use of polymeric polyphosphate stabilizers, which presumably stabilize the particles by adhering to their surfaces. Henglein's and our results, as well as the work of others,[3e,f] indicate that the coordination chemistry of nanocluster surfaces is the critical issue in nanocluster stabilization. Our sol-gel-like synthesis, exemplified by eq 3, offers the ability to vary the covalent surface substituents, and offers many reaction variables to control the overall process. Further studies are in progress to establish the generality of the procedure, and to produce optimally stabilized, highly crystalline, monodispersed nanoclusters. We are also developing related procedures using precursors that are easier to obtain and to handle.

Acknowledgment. Support to W.E.B. was provided by the donors of the Petroleum Research Fund, administered by the American Chemical Society, the Monsanto Co., and an NSF Presidential Young Investigator award. Support to M.S.C. was provided by NSF DMR-9024502. Washington University provided equipment support. The Washington University High-Resolution NMR Service Facility was funded in part by NIH Biomedical Research-Support Shared-Instrument Grant 1 S10 RR02004 and a gift from the Monsanto Co. W.E.B. is grateful to Dr. Subhash C. Goel and Professor James K. Bashkin for many helpful discussions.

Supplementary Material Available: Figures showing digitized electron diffraction and X-ray diffraction patterns of bulk and nano-Cd_3P_2 (3 pages). Ordering information is given on any current masthead page.

(16) Goel, S. C.; Viano, A. M.; Adolphi, N. L.; Stoddard, R. D.; Conradi, M. S.; Gibbons, P. C.; Buhro, W. E. Unpublished.
(17) Haase, M.; Weller, H.; Henglein, A. *Ber. Bunsen-Ges. Phys. Chem.* **1988**, *92*, 1107.

Reviews

Zeolates: A Coordination Chemistry View of Metal-Ligand Bonding in Zeolite Guest-Host Inclusion Compounds

Geoffrey A. Ozin* and Saim Özkar†

Advanced Zeolite Materials Science Group, Lash Miller Chemical Laboratories, University of Toronto, 80 Saint George Street, Toronto, Ontario, Canada M5S 1A1

Received February 12, 1992

Various guests have been investigated in zeolite hosts in our laboratory over the past five years. From analysis of in situ spectroscopic observations (FT-IR, UV-vis, Mössbauer, DOR-MAS NMR) of the reaction sequences and structural features of precursors and products (EXAFS, Rietveld refinement of powder XRD data), the molecule size cavities and channels of zeolites respectively are viewed as providing macrospheroidal and macrocylindrical, multisite multidentate coordination environments toward encapsulated guests. By thinking, in particular, about the α- and β-cages of the zeolite Y host effectively as a "zeolate" ligand composed of interconnected and perfectly organized anionic aluminosilicate "crown ether-like" rings, the materials chemist is able better to understand and exploit the reactivity and coordination properties of the zeolite internal surface for the anchoring and self-assembly of a wide range of encapsulated guests (e.g., metal atoms, metal cations, metal clusters, coordination compounds, metal carbonyls, organometallics, metal oxides, and semiconductor nanoclusters. This approach helps with the design of synthetic strategies for creating novel guest-host inclusion compounds having possible applications in diverse areas of materials science, such as size/shape selective catalysis, nonlinear optics, quantum electronics, and photonics. To present this "crown ether-zeolate ligand analogy", we will focus attention on structurally well-defined examples of metal-zeolate bonding, involving mainly metal carbonyls and molecular metal oxides, housed within the diamond network of interlaced 13-Å supercages (α-cages) of zeolite Y, mainly taken from our recent work. A coordination chemistry view of metal-zeolate bonding in intrazeolite metal organic chemical vapor deposition type precursors and semiconductor nanocluster products is presented in a separate publication.[20]

Introduction

As a result of zeolite host-guest inclusion chemistry carried out in our laboratories over the past 5 years or so, it has become apparent that the molecule size cavities and channels of zeolites respectively behave as macrospheroidal and macrocylindrical, multisite multidentate ligands in their anchoring (complexing, coordinating, stabilizing) and structure directing properties toward a wide range of imbibed metal guests (e.g., metal atoms, metal cations, metal

† Chemistry Department, Middle East Technical University, 06531 Ankara, Turkey.

0897-4756/92/2804-0511$03.00/0